Resonant aluminum nanodisk array for enhanced tunable broadband light trapping in ultrathin bulk heterojunction organic photovoltaic devices

Wu, Bo; Liu, Xinfeng; Oo, Than Zaw; Xing, Guichuan; Mathews, Nripan; Sum, Tze Chien

2012

Wu, B., Liu, X., Oo, T. Z., Xing, G., Mathews, N., & Sum, T. C. (2012). Resonant Aluminum Nanodisk Array for Enhanced Tunable Broadband Light Trapping in Ultrathin Bulk Heterojunction Organic Photovoltaic Devices. Plasmonics, 7(4), 677-684.

https://hdl.handle.net/10356/95872

https://doi.org/10.1007/s11468-012-9358-0

Resonant Aluminum Nanodisk Array for Enhanced Tunable Broadband Light Trapping in Ultra-thin Bulk Heterojunction Organic Photovoltaic Devices

Bo Wu[1], Xinfeng Liu[1], Than Zaw Oo[2], Guichuan Xing[1], Nripan Mathews[2] and Tze Chien Sum[1*]

[1]*Division of Physics and Applied Physics, School of Physical and Mathematical Sciences, Nanyang Technological University, Singapore 637371, Singapore*

[2]*Division of Materials Technology, School of Materials Science and Engineering, Nanyang Technological University, Singapore 639798, Singapore*

(Received)

A cost-effective approach to enhancing broadband light trapping in ultra-thin bulk heterojunction organic photovoltaic (OPV) devices is proposed. This is achieved by simply inserting an array of Al nanodisks at the interface of the ITO anode and the organic active layer; forming circular plasmonic nano-patch cavities (between the nanodisks and the Al cathode) that sandwich the active layer. Through interactions between the surface plasmon polaritons (SPP) localized at the nanodisk and the cathode, a tunable broadband resonance peak spanning 450 – 700 nm in the scattering cross-section spectrum is formed, thereby enhancing the electromagnetic field in the active layer. Compared to an OPV device with a 60 nm thick PCPDTBT:$PC_{60}BM$ layer, our numerical simulations reveal that integrated absorption enhancements of up to 40% can be achieved in an equivalent device integrated with an array of nanodisks with a diameter of 100 nm and a periodicity of 250 nm. From the analysis of the structure-performance relationships, implications for the design of these nano-patch cavities for light harvesting in ultra-thin OPV devices are discussed.

Keywords: organic photovoltaic device; aluminum; plasmonic cavity resonance; enhancement; ultrathin; cost-effective

* Electronic mail: tzechien@ntu.edu.sg; Tel: (65)6316 2971

Bulk heterojunction (BHJ) organic photovoltaic (OPV) devices present a promising solution to our clean and renewable energy needs. Their attractiveness include: solution processability, ease of fabrication and compatibility with flexible substrates which could enable the utilization of roll to roll printing techniques.[1] However, one major impediment to their commercial viability is their much lower power conversion efficiencies (PCE or η) compared to their inorganic counterparts, with the highest reported PCE till date of ~7-8%.[2] The main constraints to the efficiency of OPV devices are intrinsic to their material systems: high energy and narrow absorption bands limiting the light harvesting efficiency and low carrier mobilities limiting the active layer thickness. Enhancing the absorbance with a thicker active layer need not necessarily lead to an increase in η due to the concomitant increase of internal resistance and carrier recombination losses; while thin active layers are inefficient due to poor absorbance. One approach out of this predicament would be to utilize light trapping strategies [3-12] to confine light within the active layer to promote absorption, thereby increasing the optical thickness of OPV materials for light harvesting. It is highly desirable to fabricate optically thick, yet physically thin OPV devices, as this would lead to reduced materials and fabrication costs in addition to performance advantages (i.e. reduced bulk recombination leading to higher open circuit voltages, V_{OC}). To fully realize the potential of OPV devices for the next generation of cost-effective, clean, lightweight, flexible and renewable energy production, it is essential to reduce the manufacturing costs while increasing the OPV device efficiencies.[6]

Recently, there has been substantial interest in the use of plasmonic metal nanostructures in solar cells for light trapping. These light trapping approaches, aptly summarized by Atwater and Polman [13], include: (1) scattering from metal nanoparticles at the surface of the solar cell, (2) near field coupling through localized surface plasmon excitations by embedded metal nanoparticles in the solar cell, and (3) surface plasmon polariton excitations at metal/semiconductor interface to couple light into the surface plasmon polariton (SPP) or photonic modes. Several theoretical and experimental works on the improvement of η with the incorporation of plasmonic metal nanostructures have been reported. In the case of bulk heterojunction OPV devices, this usually involves their integration in the PEDOT:PSS

buffer layer or in direct contact with the active layer. Such integration could lead to an anomalous increase[14] or decrease [15] in PCE which could arise from a range of factors. Plasmonic origins to the PCE improvement can be attributed to the increased light absorption in the active layer brought about either by strong scattering and/or waveguiding by the metal nanostructures that enhances the electromagnetic (EM) field in the active layer or by overlap of the strong plasmonic modal fields with the active layer. However, losses from the metal absorption as well as that from backscattering by the metallic nanostructures (resulting in destructive Fano interference) near the surface plasmon resonances (SPRs) [16,17] could negate any enhancement, leading to low or reduced PCE [12,18]. Other non-plasmonic origins of the enhancement or detraction include: morphology changes in the active material; improved/degenerated charge injection at the electrodes; modification of the carrier mobility [15,19] and exciton quenching [20] at the bare metal surface etc. These pertinent issues highlight the formidable challenges encountered in the design and integration of plasmonic metal nanostructures in OPV architectures.

While there have been numerous reports on the utilization of Au and Ag nanostructures for plasmonic OPV devices, those on the use of aluminum (Al) are far and few [21,22]. The salient advantages of Al over Au or Ag are the cost; its compatibility with existing OPV fabrication steps (where Al is already being used as the cathode material); and its resistance to photo-degradation (unlike Ag) through the formation of a thin protective oxide layer, which could also function as a coating to reduce exciton recombination at the bare metal nanostructure surfaces. One interesting idea to enhance the resonant scattering in metal nanostructures for increased light absorption in the active layer is based on the concept of plasmonic cavity resonance (PCR). This concept leverages on the unique ability of surface plasmons to focus or confine broadband light in a nanocavity that supports the propagation of gap plasmon modes. While the PCR concept is no stranger to applications in plasmonic lasing,[23] sensing,[24] etc., this has rarely being applied to enhancing light harvesting in OPV devices. Investigating this PCR concept utilizing cost-effective Al nanodisks for enhanced tunable broadband light trapping in OPV devices is the main focus of this paper.

Herein, we report on a numerical study for a cost-effective approach to enhance broadband light trapping in thin-film bulk heterojunction OPV devices using an array of Al nanodisks inserted between the ITO anode and the organic active layer. The plasmonic nano-patch cavities[25,26] formed between the Al nanodisks and the underlying Al cathode exhibit superior light scattering properties, leading to enhanced light trapping in the ultrathin active layer. With respect to a bare OPV device with a 60 nm thick PCPDTBT:$PC_{60}BM$ (Poly[2,1,3-benzothiadiazole-4,7-diyl[4,4-bis(2-ethylhexyl) - 4H - cyclopenta [2,1-b:3,4-b']dithiophene-2,6-diyl]]:[6,6]-Phenyl-C61-butyric acid methyl ester) layer, integrated absorption enhancements up to 40% can be achieved in an equivalent device integrated with an array of nanodisks with a diameter of 100 nm and a periodicity of 250 nm. Through finite difference time domain (FDTD) simulations, we seek to gain new insights into the basic mechanism of light trapping and the physics of PCR in an OPV device. We also seek to establish the structure-performance relationships in these hybrid plasmonic-OPV devices that will enable tuning of the light harvesting properties by appropriate selection of materials (i.e. the metal species and OPV materials) and optimal structural design. Importantly, our findings suggest a viable strategy to develop cost-effective, high efficiency, ultra-thin plasmonic OPV devices.

The Physics of Plasmonic Cavity Resonance in a Nano-patch Cavity

To elucidate the principles of light trapping with a plasmonic cavity, we will first examine the simulation of a single nanodisk in a nano-patch cavity configuration (see Fig. 1(a)) before moving on to the more complicated scenario of an OPV device with an array of nanodisks. The simulation was performed using the Lumerical^{TM} FDTD software. The structure comprises of a thick Al film (i.e. the Al cathode), followed by a dielectric layer (i.e. the organic active layer) that is topped by an Al nanodisk with a diameter (D) of 60 nm and height (H) 30 nm. Overcoating this Al nanodisk is another dielectric medium which we have termed as the cladding. A disk-shaped structure was selected over a spherical one due to the stronger near-field coupling [27] of the former and its relative ease of fabrication using nanolithography techniques compared to the latter. For simplicity, the refractive indices of the dielectric

media (i.e. active layer and cladding) are also set to $n = 2$, which is comparable to the refractive indices of organic active layer and the ITO. A total field/scattered field (TFSF) source is incident on the Al nanodisk with propagation direction indicated as shown in Fig 1(a). This TFSF source is extremely useful for studying the scattering properties of particles as it allows us to numerically separate the incident field from the scattered field.

Fig. 1(b) shows the spectral dependence of the normalized scattering cross-section (Q_{scat}) for different active layer thicknesses (T). Q_{scat} is defined as the ratio of the scattered power to the product of the incident intensity with the geometrical cross section (i.e., the area of the particle projected on the substrate.[27] The scattered power is calculated by integrating the Poynting vector of the scattered field over a box enclosing the nanostructure. When T is smaller than or comparable to the diameter (D) of Al nanodisk (i.e. $T / D \leq 1$), the spectrum exhibits two distinct peaks; with one relatively narrower peak at the bluer wavelengths (i.e. ~ 400 – 420 nm) and a broader peak at the redder wavelengths. The position of the blue peak is relatively invariant to the variation in thickness of the active layer, while that of the broad peak blue shifts significantly as the active layer thickness increases. When the thickness of the dielectric layer exceeds the diameter of Al nanodisks (i.e. $T > 60$ nm), the two peaks merge. The electric field intensity distribution (in the x-z plane) for a 30 nm active layer at the scattering peaks of ~410 nm (blue peak) and ~500 nm (red peak) are shown in Fig. 2(a) and (c) respectively.

The E-field signature of the blue peak is typical of one from a quadruple plasmon resonance forming lobes at both the top and bottom edges of the nanodisk [12]. This originates from a pair of dipoles that oscillate in phase with one dipole formed near the top interface and another near the bottom interface of the Al nanodisk (see Fig. 2(a) and (b)) – i.e. a dipole-like resonance. The E-field is mainly concentrated near the bottom edge of the nanodisk, closer to cladding layer. For the red peak, the E-field intensity distribution is characteristic of the TM110 mode of a circular nano-patch cavity [25,26], with the field mainly concentrated near the top edge of the nanodisk, extending over the active layer to the Al electrode (see Fig. 2(c) and (d)). With the energy trapped mainly in the active layer, this mode would be

beneficial for light harvesting in an OPV device. To verify our deductions, further simulations were performed – one involving only the Al nanodisk (and without the Al film) surrounded by a uniform dielectric medium with $n = 2$; and another involving the implementation of an effective index n_{eff} for the active layer and the Al film in a region central to the Al nanodisk. In both cases, the dimensions of the Al nanodisk remain as $D = 60$ nm and $H = 30$ nm.

In the case of a bare Al nanodisk encapsulated in a $n = 2$ dielectric medium, there is only one localized surface plasmon resonance (LSPR) peak at ~440 nm, which is close to the value of 410 nm in our original case (i.e. with Al film). The blue shift in the LSPR peak value in the original case can be attributed to interactions between the Al nanodisk and the Al film. This is evident from Fig. 1(b) where for T / D ratios approach 1, the blue peak red shifts to a value closer to 440 nm. For thicker active layers, the interaction between the nanodisk and the film has weakened considerably and both the blue and red peaks merge to yield the LSPR peak for the case of a single Al nanodisk.

The red peak present in the original case is missing in our simulations involving only the bare Al nanodisk. To establish if its origins can be traced to the nano-patch cavity formed with the Al film, we implemented an effective refractive index approximation (ERIA) of the active layer and the Al film (in the original case) in a region central to the Al nanodisk following the procedure reported by Kuttge *et. al.* [28], which was applied for much larger disk diameters of 2 microns. For the larger disks, there is more than one resonating mode confined in the cavity. As the disk diameter shrinks to dimensions much smaller than the wavelength of the incident light, only a single mode can be sustained. [28] From the dispersion relations of a typical planar metal-insulator-metal (MIM) structure, an effective refractive index, n_{eff}, can be derived:

$$\tanh(k_d d/2) = \begin{cases} -\dfrac{\varepsilon_d k_m}{\varepsilon_m k_d} & \text{, for the anti-symmetric mode} \\ -\dfrac{\varepsilon_m k_d}{\varepsilon_d k_m} & \text{, for the symmetric mode} \end{cases} \quad \text{- (1)}$$

where $k_d = \sqrt{k_{sp}^2 - \varepsilon_d \frac{\omega^2}{c^2}} = \sqrt{n_{eff}^2 - \varepsilon_d}\,\frac{\omega}{c}$, $k_m = \sqrt{k_{sp}^2 - \varepsilon_m \frac{\omega^2}{c^2}} = \sqrt{n_{eff}^2 - \varepsilon_m}\,\frac{\omega}{c}$, d is the thickness of active layer, ε_d and ε_m are the real parts of dielectric constants of the active layer and the metal (i.e. Al film), respectively; k_d and k_m being the wavevectors of the propagating waves in the active layer and metal and and k_{sp} being the wavevector of the surface plasmons; ω being the frequency; and c being the speed of light.

Replacing the Al film and the active layer with a slab with $n_{eff}(\omega)$ in a region central to the Al nanodisk, with the nanodisk and the slab with $n_{eff}(\omega)$ now being surrounded by a n = 2 cladding layer - see Fig. 3 inset, we perform the FDTD simulations (using a cylindrical geometry for ease of computation) to obtain the spectral dependence of the Q_{scat} for the Al nanodisk. For each thickness of the active layer, an effective index must be computed from the SPP dispersion relations; from which the Q_{scat} was calculated using the FDTD simulations. To minimize the number of variables in these simulations, an average effective radius of 42 nm was fixed for the $n_{eff}(\omega)$ slab, which represents the average extent of interactions from the Al nanodisk for active layers with varying thicknesses. The slightly larger radius for the cylindrical $n_{eff}(\omega)$ slab (42 nm) than that of the nanodisk radius (30 nm) also helps to compensate for fringe effects. [29] Good correspondence in peak positions computed using the original structure (in Fig. 1) and that computed using the ERIA structure (Fig. 3 inset) was obtained and this is plotted as shown in Fig. 3. Hence, we can confirm that the red peak in Fig. 1 originate from the excitation of circular nanopatch cavity modes, likely to be that of the TM110 mode. Equivalently, it should also be noted that a recent report on the study of the surface plasmon resonances in linear nanoparticle clusters showed that the homogenization procedure used in the ERIA leads to a new plasmonic medium outside the nanoparticles, thereby creating a new localized surface plasmon

resonance mode. [30] Nonetheless, from the configuration of our structure (nanodisks rather than nanoparticles) and the resulting EM field distribution from the FDTD simulations (see Fig. 2), we feel that it may be more appropriate to use the nomenclature of plasmonic cavity resonance, in accordance to several reports found in the literature [23,24]. Our simulation results can be further validated with the results of previously reported simulations of a Ag nanodisk on top of a Si substrate with air as the cladding [31,32] – both short wavelength dipole-like free space modes at the Ag/air interface and long wavelengths modes due to geometric resonances of the SPPs at the Ag/substrate interface [32] exist. Analogously, in Fig. 3 inset, we have both the short wavelength dipole-like free space modes at the Al/cladding interface and long wavelengths modes due to geometric resonances of the SPPs at the Al/n_{eff} slab interface.

For completeness, we have also briefly examined alternative models applied in the analysis of complex plasmonic nanostructures such as the hybridization model [33] and the image charge model [34], where we found some advantages of our approach. For example, the hybridization model which considers the plasmon response as an interaction of elementary plasmons rely on the input of precise analytical solutions for the response of the constituent plasmons (i.e., the localized surface plasmon frequency of the nanodisk and the cavity plasmon frequency in our case); which is not easily obtained or almost impossible for our case. The image charge model on the other hand, considers that the interaction between the original nanostructure and its image charge (in the substrate) results in a splitting of the plasmon resonance. However, when utilizing this key idea in the simulations (i.e. replacing the Al cathode with an Al nanodisk at the image position), the outcome do not correspond well with our earlier results for the red and blue peaks. In contrast to these two alternative models, our simple ERIA approach could satisfactorily predict the peak positions of the two resonances and yield insights into the underlying physics of plasmonic cavity resonance in a nano-patch cavity.

From our FDTD simulations, it is clear that the electromagnetic (EM) energy of the dipole-like mode (i.e. the blue peak) is concentrated at the bottom of the nanodisk and far from the active layer. The

near field of this mode does not overlap significantly with the active layer, and consequently light harvesting is greatly reduced [32]. Due to the destructive interference of the incident and scattered light (i.e. Fano interference) [16,17] at the blue side of this resonance peak, optical losses will be incurred instead. In the case of an Ag nanodisk, its LSPR peak matches with the absorption bands of the active layer (i.e. ~ 500-600 nm), high loss will occur for wavelengths below this LSPR peak ($\lambda < \lambda_{LSPR}$), reducing the broadband absorption enhancement as confirmed by more simulations. Hence Ag would be not a desirable choice of material for the nanodisk for this approach to light trapping. For the cavity modes, the EM energy is strongly confined in the active layer, which is highly beneficial for light focusing or trapping in the active layer. In the case of an Au nanodisk, as its LSPR peak is already located in the red spectral region, the PCR peak is likely to be located deeper in the red. Hence, it would be completely mismatched with the absorption bands of the organic active layer. Al is therefore the most suitable metal for this light harvesting approach. Any optical losses due to the quadruple plasmon resonance mode would be minimal as this peak is located at ~ 400nm – a region where the solar spectrum exhibits relatively lower irradiance and the organic active layers exhibit weak absorbance. The Al PCR peak on the other hand can provide good spectral matching with the absorption bands of the active layer.

Plasmonic Cavity Resonance in an Organic Photovoltaic Device

With the insights gained from a simplified nanopatch cavity structure, we will next examine a more complicated scenario of an OPV device with an array of Al nanodisks to establish the structure-performance relationships in these hybrid plasmonic-OPV devices. Fig. 4(a) shows the layout for a typical OPV device where the active layer was replaced with P3HT:$PC_{60}BM$, P3HT:$PC_{70}BM$, PCPDTBT: $PC_{60}BM$, PCPDTBT: $PC_{70}BM$. Instead of a uniform cladding layer overcoating the whole Al nanodisk, the Al nanodisk now resides on the indium tin oxide (ITO) anode layer and is embedded inside a PEDOT:PSS hole-transporting layer. The refractive indices of ITO, PEDOT:PSS and polymer-PCBM blends used in our simulation are obtained from references [35-37]. The device structure (shown

in Fig. 4(a) inset which comprise only of a representative section with one Al nanodisk) is: indium-tin oxide (ITO) (200 nm) / PEDOT:PSS (20 nm) – Al nanodisks (D = 60 nm, H = 20 nm, periodicity P = 250 nm) / Active layer (various species and thickness) / Al cathode (200nm). In the direction of light propagation, the simulation region is terminated with a perfectly matched layer as the boundary condition to eliminate any spurious reflection arising from the edges of the simulation region. Periodic boundary conditions were set for the other axes. We have used the standard AM1.5 solar spectrum as the simulation source. The absorption enhancement is defined by the formula given below:

$$Enh = \frac{\int_0^\infty [\alpha(\lambda) - \alpha_0(\lambda)]\Phi(\lambda)d\lambda}{\int_0^\infty \alpha_0(\lambda)\Phi(\lambda)d\lambda} \qquad \text{- (2)}$$

where $\alpha(\lambda)$ and $\alpha_0(\lambda)$ are the absorption coefficients of the organic active layer with and without the Al nanodisks, respectively; $\Phi(\lambda)$ is the photon flux per wavelength of the AM1.5 spectrum. Therefore, $Enh < 0$ indicates a decrease of absorption for active layer while $Enh > 0$ represents an enhanced absorption. In our calculations, we have only considered the spectral region from 400 – 900nm as below 400 nm, the solar irradiance is relatively weak and above 900nm, the active layer has almost no absorption.

Fig. 4(a) shows the simulated percentage enhancement in different active layers with and without the Al nanodisks array (P = 250 nm). As the thickness of the active layer is increased from 20nm to 60nm, the absorption enhancement of all the active layers drops rapidly. Beyond the 60 nm thickness, the modal confinement of the cavity mode is so weak that any light trapping advantages afforded by the plasmonic cavity could no longer compensate for the intrinsic absorption losses and back-scattering losses from the Al nanodisks. This is in agreement with the earlier trend (i.e. $T / D \leq 1$) shown in Fig. 1(b) where the Q_{scat} spectrum exhibits two distinct peaks. This clearly shows the significance of the plasmonic cavity confinement in such circular plasmonic nano-patch cavity configuration. Once the plasmonic cavity confinement weakens and disappears, there will be little enhancement to the absorption. Our simulations also show that the PCPDTBT:PC_{60}BM active layer

exhibits the best light trapping properties over the range 45 – 70 nm active layer thickness. This can be attributed to its lower absorption coefficient which results in a less lossy plasmonic resonance and thus better light trapping.

Next, we shall focus on a 60 nm thick PCPDTBT: $PC_{60}BM$ active layer while varying the periodicity of the Al nanodisks. As the periodicity of the nanodisk array is increased from 100 – 500 nm, the absorption enhancement increases and peaks at about 250 nm as shown in Fig. 4(b). This is because the effective cross section of the plasmonic particle is much larger than its geometrical cross section due to its strong scattering.[12] At high nanodisk densities (exceeding a critical value), the optical losses due to the plasmon resonance at the blue side would be very strong, thus negating the benefits of increased absorption brought about by scattering and cavity confinement. On the other hand, as the periodicity increases, the particle density will decrease and the light confined by the cavity per unit area will decrease; resulting in a decrease in absorption enhancement. Our simulations show that an intermediate value of about 250nm is optimal for light trapping.

With these insights on the thickness of the active layer and the periodicity of the nanodisk array, we seek to establish the optimal design parameters for an ultrathin OPV device with a 60 nm thick PCPDTBT: $PC_{60}BM$ active layer. While maintaining the nanodisk periodicity at 250 nm, we seek to increase the light trapping properties with larger Al nanodisks. As D is increased, Fig. 5(a) shows that broadband enhancement in the absorbed photon numbers over a spectral range of 400 to 900 nm. Importantly, in the absence of the Al cathode (i.e. no plasmonic cavity formed), this broadband enhancement is absent (see Fig. 5(b)). As D is increased from 60 nm to 80 nm and 100 nm, the corresponding absorption enhancement was calculated to be 9.48%, 27.01%, and 40.85% respectively. Further increase of D leads to a gradual decrease of the enhancement (not shown for clarity of the enhancement in the spectrum for the above cases). This is attributed to the following reasons: (1) a shadowing effect by the larger nanodisks which negate the light trapping advantages and (2) a mismatch of the PCR peak with the absorption bands of the active layer. This latter effect can be seen from Fig.

1(b) where both the dipole-like (blue) peak and the PCR (red) peak redshifts as the ratio of T/D is reduced (i.e. here T is fixed at 60 nm), leading a spectral mismatch of the latter peak with the absorption bands and to a limited extent, a spectral matching of the former peak with the absorption bands. As discussed previously, spectral matching of the dipole-like (blue) peak with the absorption bands of the active layer is undesired as this would lead to further optical losses. Hence, the optimal D for an active layer T = 60 nm is approximately 100 nm. Fig. 5(a) inset shows the electric field intensity distributions (in log scale) in the $x - z$ plane for the red PCR peak for nanodisks of different diameters, with the D = 100 nm exhibiting the most intense interactions with the Al cathode.

Lastly, to provide a better estimation of the performance of our design under more realistic and practical nano-fabrication conditions (i.e. costs/difficulty considerations), we simulated the cases where: (a) the fabricated nanodisks are less than perfect nanostructures – e.g. with oblate spheroids which may be cheaper and easier to fabricate; (b) the deviation of the periodicity of the array from the design; and (c) the presence of some disorder in the nanodisk array. For (a), we replace the "perfect" nanodisks (i.e., radius: 50 nm, height: 20 nm, periodicity: 300 nm) with oblate spheroids (i.e., major axis: 50 nm, minor axis: 10 nm, periodicity: 300 nm). A weaker enhancement of 17.44% could still be achieved. This decrease in absorption enhancement can be mainly ascribed to the curved surface of the spheroid, which inhibits the formation of strong cavity resonance with the Al cathode unlike the nanodisk. For (b), our simulations indicate that the periodicity of the nanodisks has less of an effect on the absorption enhancement. Using nanodisks with radius: 50 nm and height: 20 nm as an example, absorption enhancements >20% could still be achieved despite varying the periodicity from ~200 nm to 450 nm. For (c), we considered a disturbed (quasi-periodic) array for which the nanodisk center deviate randomly from the periodic array (periodicity: 300 nm), using a Gaussian distribution with positional standard deviation of 50 nm. Our simulations show that an average absorption enhancement as high as 38.44% could still be achieved, which is close to the optimized periodicity. A final word on the fabrication of these plasmonic nanostructures – one could turn to nanoimprint lithography and metal evaporation to fabricate these large-area periodic arrays with relatively cost-effectiveness, high

throughput and high resolution. These results clearly demonstrate the viability of this cost-effective approach to enhancing broadband light trapping in ultra-thin bulk heterojunction organic photovoltaic (OPV) devices.

Conclusions

In summary, we have proposed a cost-effective approach for enhanced broadband light trapping in thin-film bulk heterojunction OPV devices. This is simply achieved by inserting an array of Al nanodisks between the ITO anode and the organic active layer at an appropriate distance from the Al cathode. Plasmonic nanocavities formed between Al nanodisks and the underlying Al cathode exhibit superior light trapping properties, leading to enhanced absorption in the ultrathin active layer in the gap. The basic mechanism of light trapping and the physics of PCR in the MDM structure of an OPV device were investigated using numerical simulations. We have also established the structure-performance relationships for these hybrid plasmonic-OPV devices that will enable tuning of their light harvesting properties by appropriate selection of materials (i.e. the metallic species and OPV materials) and optimal structural design. Importantly, our findings suggest a viable strategy to develop cost-effective, high efficiency, ultra-thin plasmonic OPV devices that are also highly relevant for hybrid thin film organic-inorganic photovoltaic devices.

Acknowledgements

The work is supported by the Singapore National Research Foundation through the Competitive Research Programme under Project No. NRF-CRP5-2009-04 (X. Liu and T. C. Sum). T. C. Sum acknowledges the financial support from the Nanyang Technological University start-up grant (M58110068) and from the Ministry of Education (MOE) Academic Research Fund (AcRF) Tier 1 grant – RG 49/08 (M52110082).

REFERENCES

1. Park SH, Roy A, Beaupre S, Cho S, Coates N, Moon JS, Moses D, Leclerc M, Lee K, Heeger AJ (2009) Bulk heterojunction solar cells with internal quantum efficiency approaching 100%. Nat Photon 3 (5):297-302. doi:http://www.nature.com/nphoton/journal/v3/n5/suppinfo/nphoton.2009.69_S1.html
2. Liang Y, Xu Z, Xia J, Tsai S-T, Wu Y, Li G, Ray C, Yu L (2010) For the Bright Future—Bulk Heterojunction Polymer Solar Cells with Power Conversion Efficiency of 7.4%. Advanced Materials 22 (20):E135-E138. doi:10.1002/adma.200903528
3. Tumbleston JR (2009) Electrophotonic enhancement of bulk heterojunction organic solar cells through photonic crystal photoactive layer. Appl Phys Lett 94 (4):043305
4. Tumbleston JR, Ko D-H, Samulski ET, Lopez R (2009) Absorption and quasiguided mode analysis of organic solar cells with photonic crystal photoactive layers. Opt Express 17 (9):7670-7681
5. Ko D-H, Tumbleston JR, Zhang L, Williams S, DeSimone JM, Lopez R, Samulski ET (2009) Photonic Crystal Geometry for Organic Solar Cells. Nano Letters 9 (7):2742-2746. doi:10.1021/nl901232p
6. Agrawal M, Peumans P (2008) Broadband optical absorption enhancement through coherent light trapping in thin-film photovoltaic cells. Opt Express 16 (8):5385-5396
7. Tvingstedt K, Dal Zilio S, Inganäs O, Tormen M (2008) Trapping light with micro lenses in thin film organic photovoltaic cells. Opt Express 16 (26):21608-21615
8. Gjessing J, Marstein ES, Sudbø A (2010) 2D back-side diffraction grating for improved light trapping in thin silicon solar cells. Opt Express 18 (6):5481-5495
9. Niggemann M, Riede M, Gombert A, Leo K (2008) Light trapping in organic solar cells. physica status solidi (a) 205 (12):2862-2874. doi:10.1002/pssa.200880461
10. Gombert A (2004) Some application cases and related manufacturing techniques for optically functional microstructures on large areas. Opt Eng 43 (11):2525
11. Kulkarni AP, Noone KM, Munechika K, Guyer SR, Ginger DS (2010) Plasmon-Enhanced Charge Carrier Generation in Organic Photovoltaic Films Using Silver Nanoprisms. Nano Letters 10 (4):1501-1505. doi:10.1021/nl100615e
12. Diukman I, Tzabari L, Berkovitch N, Tessler N, Orenstein M (2011) Controlling absorption enhancement in organic photovoltaic cells by patterning Au nano disks within the active layer. Opt Express 19 (S1):A64-A71
13. Atwater HA, Polman A (2010) Plasmonics for improved photovoltaic devices. Nat Mater 9 (3):205-213
14. Kim C-H, Cha S-H, Kim SC, Song M, Lee J, Shin WS, Moon S-J, Bahng JH, Kotov NA, Jin S-H (2011) Silver Nanowire Embedded in P3HT:PCBM for High-Efficiency Hybrid Photovoltaic Device Applications. ACS Nano 5 (4):3319-3325. doi:10.1021/nn200469d
15. Xue M (2011) Charge-carrier dynamics in hybrid plasmonic organic solar cells with Ag nanoparticles. Appl Phys Lett 98 (25):253302
16. Beck FJ (2009) Tunable light trapping for solar cells using localized surface plasmons. J Appl Phys 105 (11):114310
17. Ferry VE, Verschuuren MA, Li HBT, Verhagen E, Walters RJ, Schropp REI, Atwater HA, Polman A (2010) Light trapping in ultrathin plasmonic solar cells. Opt Express 18 (S2):A237-A245
18. Tsai S-J, Ballarotto M, Romero DB, Herman WN, Kan H-C, Phaneuf RJ (2010) Effect of gold nanopillar arrays on the absorption spectrum of a bulk heterojunction organic solar cell. Opt Express 18 (S4):A528-A535
19. Kim K (2005) Roles of Au and Ag nanoparticles in efficiency enhancement of poly(3-octylthiophene)/C60 bulk heterojunction photovoltaic devices. Appl Phys Lett 87 (20):203113
20. Topp K, Borchert H, Johnen F, Tunc AV, Knipper M, von Hauff E, Parisi J, Al-Shamery K (2009) Impact of the Incorporation of Au Nanoparticles into Polymer/Fullerene Solar Cells†. The Journal of Physical Chemistry A 114 (11):3981-3989. doi:10.1021/jp910227x
21. Kochergin V (2011) Aluminum plasmonic nanostructures for improved absorption in organic photovoltaic devices. Appl Phys Lett 98 (13):133305
22. Akimov Y, Koh W (2011) Design of Plasmonic Nanoparticles for Efficient Subwavelength Light Trapping in Thin-Film Solar Cells. Plasmonics 6 (1):155-161. doi:10.1007/s11468-010-9181-4

23. Zhu X, Zhang J, Xu J, Yu D (2011) Vertical Plasmonic Resonant Nanocavities. Nano Letters 11 (3):1117-1121. doi:10.1021/nl104024j
24. Ameling R (2010) Cavity-enhanced localized plasmon resonance sensing. Appl Phys Lett 97 (25):253116
25. Manolatou CR, F.; (2008) Subwavelength Nanopatch Cavities for Semiconductor Plasmon Lasers IEEE Journal of Quantum Electronics 44 (5):435 - 447 doi:10.1109/JQE.2008.916707
26. Amit ML, et al. (2011) Lasing in subwavelength semiconductor nanopatches. Semiconductor Science and Technology 26 (1):014013
27. Catchpole KR (2008) Design principles for particle plasmon enhanced solar cells. Appl Phys Lett 93 (19):191113
28. Kuttge M, García de Abajo FJ, Polman A (2009) Ultrasmall Mode Volume Plasmonic Nanodisk Resonators. Nano Letters 10 (5):1537-1541. doi:10.1021/nl902546r
29. Balanis CA Antenna Theory - Analysis and Design (3rd Edition). John Wiley & Sons,
30. Sandu T, Vrinceanu D, Gheorghiu E (2011) Surface Plasmon Resonances of Clustered Nanoparticles. Plasmonics 6 (2):407-412. doi:10.1007/s11468-011-9218-3
31. Hägglund C (2008) Electromagnetic coupling of light into a silicon solar cell by nanodisk plasmons. Appl Phys Lett 92 (5):053110
32. Beck FJ, Verhagen E, Mokkapati S, Polman A, Catchpole KR (2011) Resonant SPP modes supported by discrete metal nanoparticles on high-index substrates. Opt Express 19 (S2):A146-A156
33. Prodan E, Radloff C, Halas NJ, Nordlander P (2003) A Hybridization Model for the Plasmon Response of Complex Nanostructures. Science 302 (5644):419-422. doi:10.1126/science.1089171
34. Vernon KC, Funston AM, Novo C, Gómez DE, Mulvaney P, Davis TJ (2010) Influence of Particle−Substrate Interaction on Localized Plasmon Resonances. Nano Letters 10 (6):2080-2086. doi:10.1021/nl100423z
35. Hoppe H, Sariciftci NS, Meissner D (2002) Optical constants of conjugated polymer/fullerene based bulk-heterojunction organic solar cells. Molecular Crystals and Liquid Crystals 385 (1):113-119. doi:10.1080/713738799
36. Monestier F, Simon J-J, Torchio P, Escoubas L, Flory F, Bailly S, de Bettignies R, Guillerez S, Defranoux C (2007) Modeling the short-circuit current density of polymer solar cells based on P3HT:PCBM blend. Solar Energy Materials and Solar Cells 91 (5):405-410. doi:10.1016/j.solmat.2006.10.019
37. Dennler G (2007) Design of efficient organic tandem cells: On the interplay between molecular absorption and layer sequence. J Appl Phys 102 (12):123109

FIGURE CAPTIONS

Fig. 1: (a) Schematics of the simulated structure with a single Al nanodisk in a nano-patch cavity configuration in isometric view and in planar cross-sectional view. (b) The spectra for the normalized scattering cross-section exhibits two distinct peaks when the thickness T is smaller than the diameter of nanodisk D. The Al nanodisk with diameter D = 60nm and height H = 30 nm, is surrounded by the active layer (n = 2) and the cladding (also set at n = 2).

Fig. 2: Electric field intensity distribution (in log scale) in the $x - z$ plane for (a) the blue peak and (c) the red peak. A simplified schematic showing the direction of the field and the location of the corresponding surface charges for (b) the blue peak which takes on the characteristics of the quadruple plasmon resonance mode (i.e. a pair of symmetric dipoles or dipole-like resonance) and (d) the red peak which takes on the chracteristics of the TM110 mode of a circular nano-patch cavity.

Fig. 3: Simulated peak positions of the blue and red maxima using the original structure shown in Fig. 1(a) and that of the ERIA structure shown in the inset for various active layer thicknesses. The dimensions of the Al nanodisk is D = 60 nm and H = 30 nm.

Fig. 4 (a) A graph of absorption enhancement (in percent) versus different active layer thicknesses for various active layer materials. Inset shows a schematic of a representative section of the hybrid OPV device with one Al nanodisk. An array of Al nanodisks with a periodicity P = 250 nm was used in this simulation. (b) A graph of PCPDTBT:$PC_{60}BM$ absorption enhancement (in percent) as a function of the Al nanodisk periodicity. For all the simulations in (a) and (b), the Al nanodisk's parameters used are: D = 60nm, H = 20nm.

Fig. 5 (a) Absorption enhancement in the PCPDTBT: $PC_{60}BM$ active layer with different Al nanodisk diameters. Inset shows the electric field intensity distributions (in log scale) in the $x - z$ plane for the red peak for nanodisks of different diameters. (b) In the absence of the Al cathode, the plasmonic cavity would not exist and any enhancement due to this plasmonic cavity would also vanish. The y axes of these graphs are normalized to the photon density of an AM 1.5 solar spectrum.

Figure 1

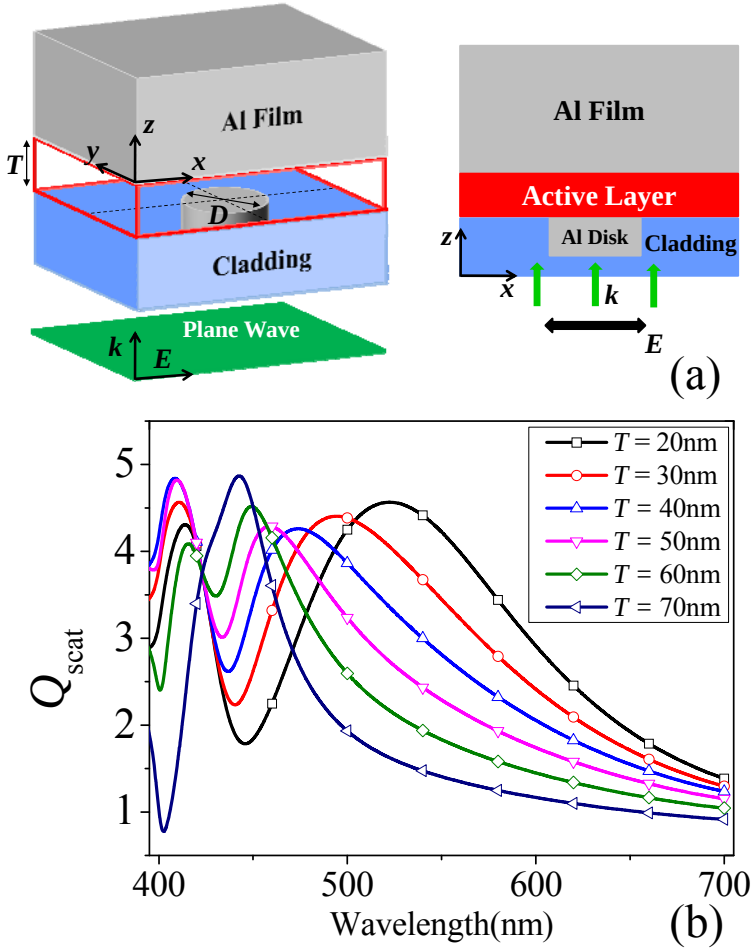
Al Film
z
y
x
T
D
Cladding
Plane Wave
k
E
Al Film
Active Layer
Al Disk
Cladding
z
x
k
E
(a)
T = 20nm
T = 30nm
T = 40nm
T = 50nm
T = 60nm
T = 70nm
Q scat
1
2
3
4
5
400
500
600
700
Wavelength(nm)
(b)

Figure 2

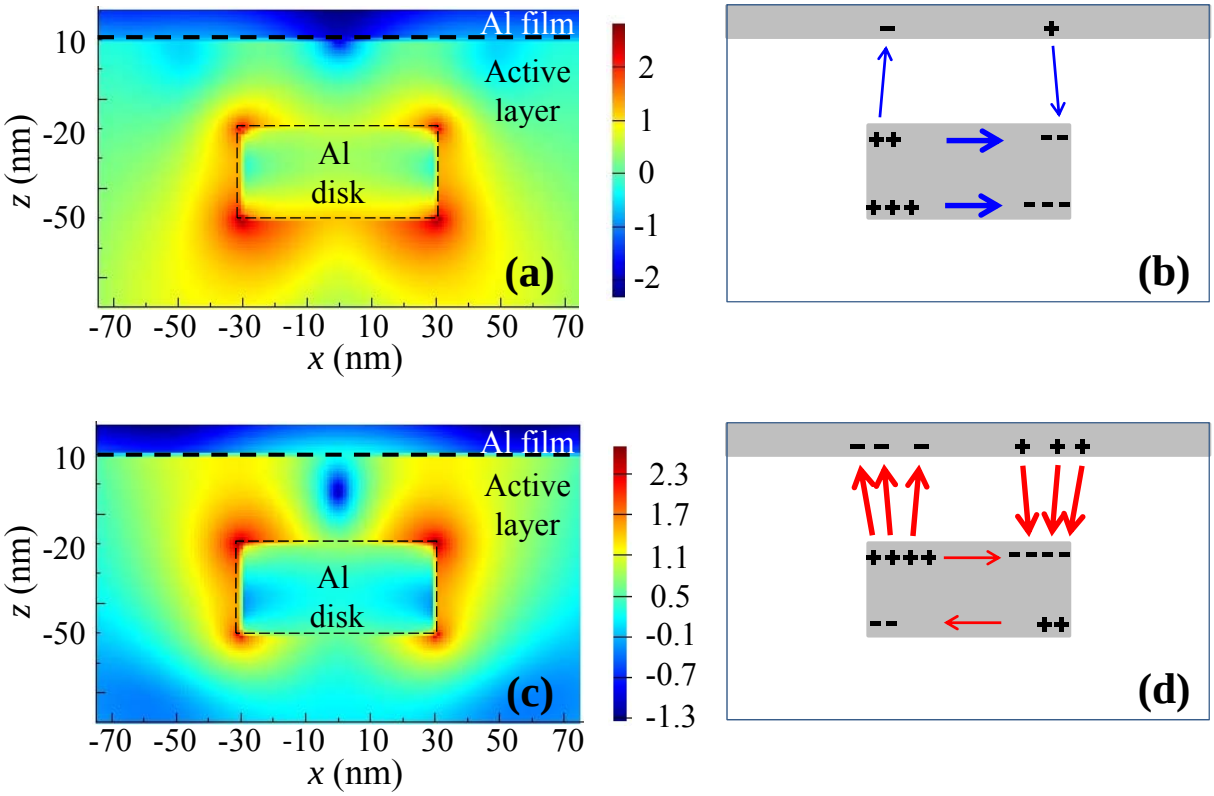
Al film
Active layer
Al disk
(a)
10
-20
-50
z (nm)
-70 -50 -30 -10 10 30 50 70
x (nm)
2
1
0
-1
-2
(b)
Al film
Active layer
Al disk
(c)
2.3
1.7
1.1
0.5
-0.1
-0.7
-1.3
(d)

Fig 3

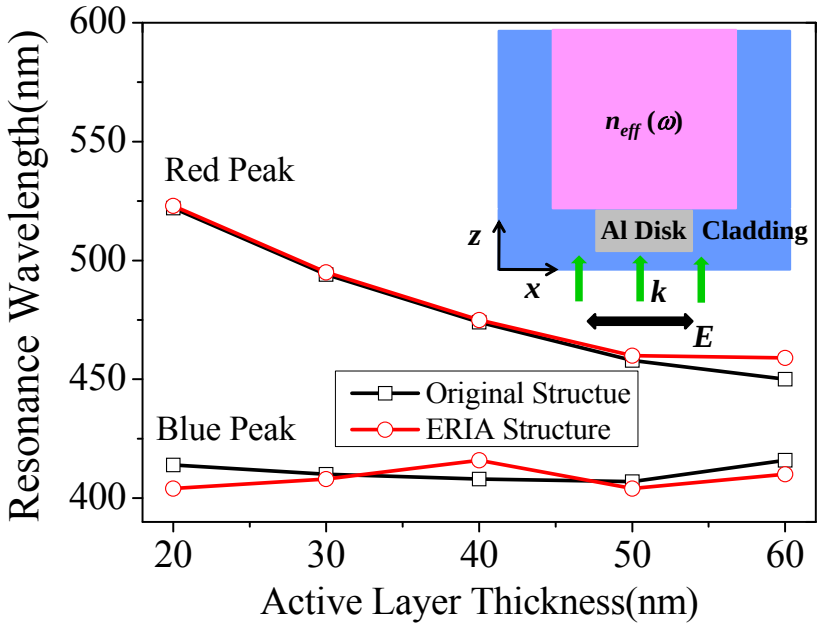
600
550
500
450
400
Resonance Wavelength(nm)
20
30
40
50
60
Active Layer Thickness(nm)
Red Peak
Blue Peak
Original Structue
ERIA Structure
$n_{eff}(\omega)$
Al Disk
Cladding
z
x
k
E

Fig 4

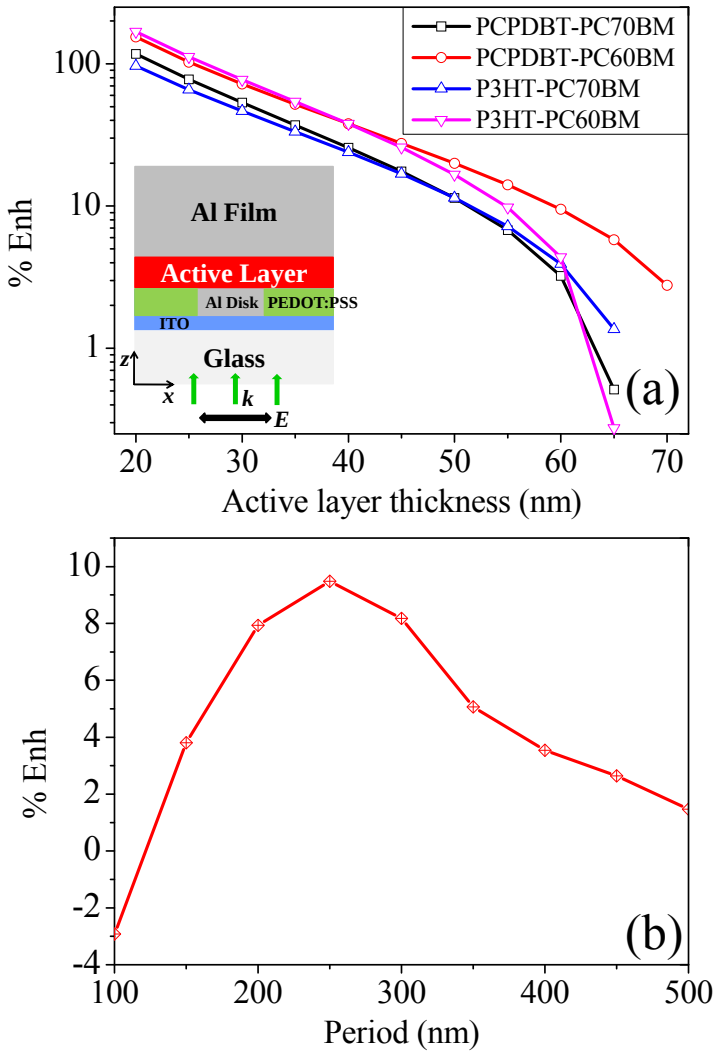
PCPDBT-PC70BM
PCPDBT-PC60BM
P3HT-PC70BM
P3HT-PC60BM
Al Film
Active Layer
Al Disk
PEDOT:PSS
ITO
Glass
z
x
k
E
(a)
% Enh
Active layer thickness (nm)
(b)
% Enh
Period (nm)

Fig 5

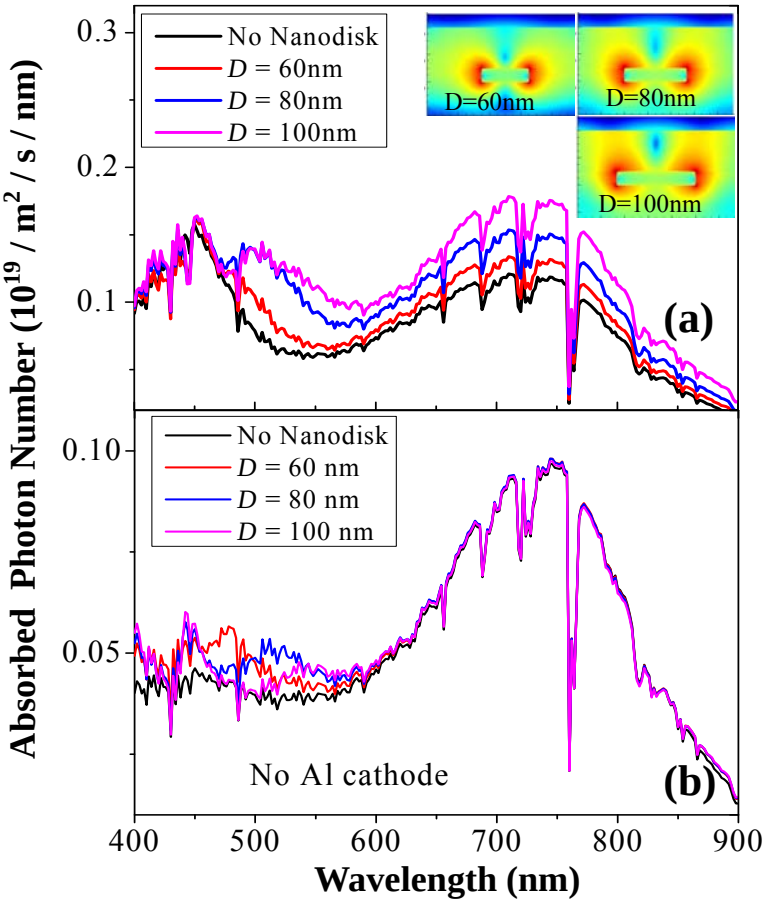
No Nanodisk
D = 60nm
D = 80nm
D = 100nm
D=60nm
D=80nm
D=100nm
(a)
No Nanodisk
D = 60 nm
D = 80 nm
D = 100 nm
No Al cathode
(b)
Absorbed Photon Number (10^19 / m^2 / s / nm)
Wavelength (nm)
0.3
0.2
0.1
0.10
0.05
400
500
600
700
800
900